ACS Catalysis

Research Article

pubs.acs.org/acscatalysis

Theoretical and Experimental Studies of C–C versus C–O Bond Scission of Ethylene Glycol Reaction Pathways via Metal-Modified Molybdenum Carbides

Weiting Yu,[†] Michael Salciccioli,[†] Ke Xiong,[†] Mark A. Barteau,[†] Dionisios G. Vlachos,*[,†] and Jingguang G. Chen*[,‡]

[†]Catalysis Center for Energy Innovation (CCEI), Department of Chemical and Biomolecular Engineering, University of Delaware, Newark, Delaware 19716, United States

[‡]Department of Chemical Engineering, Columbia University, New York, New York 10027, United States

Supporting Information

ABSTRACT: Designing catalysts with high activity and selectivity for biomass conversion to fuels and chemicals requires the understanding and controlling of the bond scission mechanism in biomass derivatives. In the current study, ethylene glycol, the smallest polyol from cellulose with the same atomic C/O ratio as C5 and C6 sugars, is employed as a surrogate molecule for controlling the bond scission sequence of O–H, C–H, C–O, and C–C bonds. A promising methodology for catalyst design is established in this work by constructing a microkinetic model to predict the activity and selectivity for ethylene glycol transformation reactions on molybdenum carbide (Mo_2C) and metal-modified Mo_2C surfaces, followed by supplementing the theoretical prediction with temperature program desorption (TPD) and high-resolution electron energy loss spectroscopy (HREELS) experiments on model surfaces. The fundamental insights from the theoretical approach and experimental results thus helps to guide the catalyst design and reduce the number of catalyst candidates in future experiments.

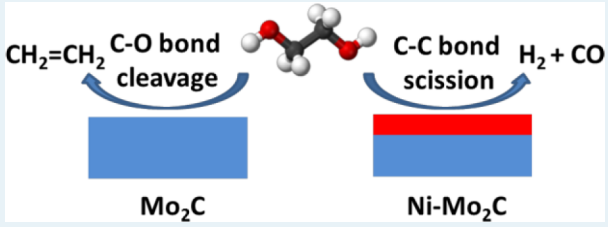

KEYWORDS: *catalyst design, microkinetic model, temperature program desorption (TPD), metal (Ni, Au, Cu, and Pt)-modified Mo_2C surfaces, biomass derivatives, ethylene glycol*

1. INTRODUCTION

Biomass-derived molecules are regarded as an alternative energy source to fossil fuels because of the advantages of being widely available, renewable, and potentially carbon-neutral. Derivatives of biomass generally contain some oxygen atoms that are not found in petroleum-based feedstocks, and therefore deoxygenation and reforming reactions are taken as two desirable chemical routes for converting biomass derivatives to chemicals and fuels. The design of effective catalysts for biomass conversion requires the understanding and controlling of the bond scission mechanisms in biomass-derived molecules. Ethylene glycol, the smallest polyol with the same atomic C/O ratio as C5 and C6 sugars, is employed as a model compound for biomass-derived molecules in this work. Another reason for choosing ethylene glycol is that a previous study has shown the direct catalytic conversion of cellulose[1] to ethylene glycol with high yield. The activity and selectivity of the ethylene glycol deoxygenation reaction to form ethylene, an important building block for commodity petrochemicals, and the reforming reaction to produce synthesis gas (H_2 and CO) will be used as probe reactions to achieve selective bond scission.

It is critical to design a catalyst with high activity, selectivity, stability as well as low cost. The reforming reaction of ethylene glycol has been studied on different 3d/Pt bimetallic surfaces,[2,3] and the monolayer (ML) 3d metal on Pt (3d-Pt) surface is identified to show higher activity than either of the parent metals. However, the favorable 3d-Pt bimetallic structure for ethylene glycol reforming is not stable at high temperatures because of the diffusion of surface 3d atoms into the Pt bulk.[4,5] Transition metal carbides have been reported in previous studies[6−9] to exhibit similar electronic properties to Pt and are 3 orders of magnitude less expensive than Pt. Molybdenum carbide (Mo_2C) is of low cost, easy to synthesize, and can serve as a diffusion barrier to metal adlayers, allowing for catalyst stability under working conditions. Mo_2C has also been reported to catalyze the deoxygenation of propanal through C–O bond scission.[10] In this work, clean Mo_2C and different admetal (Ni, Au, Cu, and Pt)-modified Mo_2C surfaces are chosen for catalyst design for ethylene glycol reactions.

The searching of active and selective catalysts for ethylene glycol reactions can be time- and effort-consuming. Although Sabatier's principle and the associated volcano curve have shaped over the years our thinking toward catalysts of optimal properties, it is important to realize that the same principles of

Received: January 27, 2014
Revised: March 20, 2014
Published: March 28, 2014

   dx.doi.org/10.1021/cs500124n | ACS Catal. 2014, 4, 1409−1418

atomic or molecular binding energies manifesting themselves into the rates of elementary surface reactions can also guide catalyst design in terms of selectivity. That is, the competitive and often convoluted pathways of the reaction network that control the observed reaction flux from reactant to different products are related to the relative forces between the bonding atoms of adsorbates and the catalyst surface. Density functional theory (DFT) parameterized microkinetic models for complex reaction networks, such as that of ethylene glycol reforming, are possible.[11] However, for mechanisms consisting of hundreds of reactions, such as the case in the current study, exploring multiple surfaces in such detail is prohibitive computationally. In addition, prior work has focused on a limited number of reaction steps of C−C bond cleaving reactions describing reforming activity. As a result, models that can predict the competing deoxygenation process for production of hydrocarbons for fuels are currently lacking. Computational screening of novel materials to predict selectivity of complex mechanisms requires a shift in the computational approach. In this work, a robust methodology for catalyst design is demonstrated by constructing an extendable, semiempirical, microkinetic model to predict not just the catalyst activity trend but also the selectivity across many surfaces. This initial semiempirical model identifies catalyst surfaces of interest, which are subsequently re-examined via DFT to elucidate divergent elementary reactions that determine product selectivity. Our computational work is complemented by temperature program desorption (TPD) experiments to confirm the predicted activity trends on clean Mo_2C and admetal (Ni, Au, Cu and Pt)-modified Mo_2C surfaces as well as the well-studied Ni/Pt(111) surfaces and HREELS experiments to verify the surface adsorbates and reaction intermediates.

2. METHODS AND TECHNIQUES

2.1. Computational Methods. A hierarchical methodology was used in this work to optimize the balance between computation cost and information gained.[12] There are three computational contributions to this work. The first one utilized a semiempirical microkinetic model to initially explore the relative activity and selectivity trends on metal-modified Mo_2C surfaces. Subsequently, reaction energies of the initial O−H bond breaking reactions (important to observed TPD activity) were calculated to further conceptualize the observed trends. Finally, because of the unique properties displayed on bare Mo_2C, further computational resources were invested to calculate reaction and activation energies of full reaction pathways leading to the observed products. It is our belief that this approach maximizes the fundamental insights gained in the work while minimizing the computational burden.

As mentioned above, to probe the reforming activity and selectivity of clean Mo_2C and monolayer admetal modified Mo_2C catalyst surfaces, a TPD microkinetic model was constructed that can predict activity and selectivity of ethylene glycol decomposition as a function of atomic binding energy descriptors. The initial construction of this model is fully described in a previous publication.[11] This model correlates atomic binding energies to molecular binding energies through metal transferable linear scaling relationships,[13−15] then relates transition state properties to intermediate properties through linear free energy relationships.[11] The major difference here is the application of the TPD design equation to the kinetic model. In addition, other details and minor changes to the semiempirical model employed in this work are described herein. All simulations start with an initial ethylene glycol coverage of 0.5 ML, consistent with experimental results. Because of the high surface concentrations of ethylene glycol at low temperatures in the TPD system, a small attractive adsorbate−adsorbate interaction was included to capture the attractive interactions of the hydroxyl groups of neighboring oxygenates. The included interaction is 5 kcal/mol/coverage/hydroxyl pair, consistent with hydrogen bonding interactions of adsorbed polyols calculated in a previous study.[15] For example, a surface with a starting coverage of 0.5 ML ethylene glycol would stabilize ethylene glycol by 2.5 kcal/mol.

This semiempirical approach was used to probe the activity and selectivity trends on several metal-modified Mo_2C surfaces. DFT calculated atomic binding energies on β-$Mo_2C(0001)$ surface and the four metal (Ni, Au, Cu and Pt)-modified surfaces as inputs to the kinetic model were obtained using the VASP code.[16,17] The lattice constants of β-$Mo_2C(0001)$ surface were a = 6.022 Å, b = 4.725 Å, and c = 5.195 Å, the same as the previous reports.[18] Ultrasoft pseudopotentials were employed to represent the interactions between ionic core and valence electrons. The PW91[19] form of the general gradient approximation (GGA) exchange correlation functional was utilized. The Brillouin zone integration was performed on a $(4 \times 4 \times 1)$ Monkhorst−Pack k-point mesh, and the cutoff energy for the plane-wave basis was fixed to 390 eV. All structure optimization and energy calculations were converged to a maximum force tolerance of 0.05 eV/Å. Spin polarization was included for the gaseous species calculations and for the Ni−Mo_2C surface. It should be noted that the real metal modified surfaces likely are not the exact geometry used here, and a perfect 1:1 mapping of the admetal to the Mo_2C substrate over the entire surface is unlikely. Nevertheless, this section serves as a starting point to understand the impact of admetal on observed product evolution through systematic changes in elementary reaction energies.

Next, adsorption of $HOCH_2CH_2OH$* and $HOCH_2CH_2O$* was modeled on a 2 × 2 slab. Although this cell size would normally be considered too small for this sized adsorbate, this configuration was chosen to better represent the ∼0.5 ML coverage of the TPD experiments. These calculations were performed to gain further insight into the trends demonstrated by the semiempirical model. These reaction energies were not used as inputs into the semiempirical model described above; rather they serve as a supplement in conceptualizing the demonstrated reactivity trends as a function of elementary reaction energy.

As part of the hierarchical modeling approach, more extensive calculations were conducted to understand the deoxygenation selectivity of ethylene glycol on the Mo_2C surface. To study the β-$Mo_2C(0001)$ surface in more detail, slightly different calculation methods were utilized (consistent with previous work[10]). For these calculations, the exchange and correlation energies were calculated using the Perdew−Burke−Ernzerhof (PBE) form of the GGA.[20] The core electron interactions were described using the projector-augmented-wave (PAW) pseudopotentials[21] with a plane-wave basis set cutoff energy of 390 eV. The surface was simulated using a 6-layer-deep (3 layers of Mo and 3 layers of C) 4 × 4 supercell with ∼16 Å of vacuum between each infinite slab in the z direction. A k-point mesh of 2 × 2 × 1 was used, all surface layers were frozen, and the adsorbate or transition state atoms were allowed to fully relax. Calculations did not include spin polarization. Previous calculations have shown these methods to be adequate for converged energy calculations.[10] Transition states were located using the dimer[22] method with initial structures for the transition state obtained

dx.doi.org/10.1021/cs500124n | ACS Catal. 2014, 4, 1409−1418

using the constrained optimization method described previously.[23,24]

2.2. Experimental Techniques. The ethylene glycol (Sigma-Aldrich, 99.8%) sample was transferred into glass sample cylinders and purified using repeated freeze−pump−thaw cycles. All other gases—hydrogen, oxygen, neon, ethylene, and carbon monoxide—were of research purity and used without further purification. The purity of all the chemicals was verified using mass spectrometry before usage. The ethylene glycol sample was dosed to the surface through a 0.7-cm-diameter stainless steel tube about 10 cm away facing the center of the surface with the exposure indicated in Langmuirs (L, 1 L = 1×10^{-6} Torr × s). The TPD and HREELS experiments were performed in two separate ultrahigh vacuum chambers with a base pressure of 2×10^{-10} Torr, as described previously.[25] A molybdenum (110) single crystal (Princeton Scientific, 99.99%, 2 mm thick and 10 mm in diameter) was attached to two tantalum posts, through which it could be heated resistively and cooled with liquid nitrogen. The temperature of Mo(110) was measured with a chromel−alumel K type thermocouple welded onto the back of the sample. The Mo_2C surface was prepared by dosing ethylene into the chamber when the surface temperature of the Mo crystal was at 600 K, followed by annealing to 1200 K, as described previously.[26] Different metal (Ni, Pt, Cu or Au)-modified Mo_2C surfaces were achieved through physical vapor deposition by controlling the current of a metal evaporation source and deposition time. Auger electron spectroscopy measurements were performed to verify the desirable metal coverages.[27] TPD experiments were performed between 105 and 800 K at a linear heating rate of 3 K/s. All possible products were monitored simultaneously using a quadrupole mass spectrometer (UTI 100C).

3. RESULTS

3.1. Reaction Activity Prediction from the Semi-empirical Model. The microkinetic model was first employed to estimate the TPD reforming activity of noble-metal-monolayer-modified Mo_2C catalyst surfaces. Results of these calculations are summarized in Table 1. DFT calculated atomic binding energies are shown with the corresponding TPD model predicted total activity and reforming activity, calculated from product desorption rates as in the experimental work. In addition, the net reaction energy of alkoxide formation from gas-phase ethylene glycol is shown as an indicator of O−H bond scission activity. The TPD reforming activity predicted by the model is a strong function of the atomic oxygen binding energy. This is traced back to the dependency of the ethylene glycol binding energy on the atomic oxygen binding energy[11] as well as the affinity of alkoxide formation as a function of oxygen binding energy.[11,15,28,29] The competition of this reaction versus the desorption energy of ethylene glycol is vital to total TPD activities because once an ethylene glycol molecule desorbs, it is no longer available for reaction and product evolution. Near-linear relationships are observed for the molecular heat of chemisorption of ethylene glycol and net reaction energy for O−H bond scission with atomic oxygen binding energy, as shown in Figure 1. Adsorption of ethylene glycol typically occurs through interactions between both hydroxyl groups and the catalyst surface.[15]

Table 1. TPD Kinetic Model Results of Ethylene Glycol Decomposition As a Function of C, O, and H Atomic Binding Energy for Pt, Ni/Pt and Monolayer Metal Mo_2C Surfaces

	atomic binding energies (kcal/mol)				TPD model predictions	
surface	C_{BE}	O_{BE}	H_{BE}	O−H net reaction energy[b] (kcal/mol)	total activity (ML)	reforming activity (ML)
Pt[a]	165	90	56	−3.3	0.037	0.037
Ni−Pt[a]	162	119	61	−26.1	0.154	0.154
Pt−Mo_2C	143	80	54	10.7	0.004	0.000
Au−Mo_2C	90	64	42	25.6	0.000	0.000
Cu−Mo_2C	137	108	55	−12.3	0.003	0.003
Ni−Mo_2C	165	114	62	−28.2	0.250	0.250
Mo_2C	176	161	76	−71.5	0.250	0.003

[a]Binding energies and net reaction energies taken from literature.[11] [b]O−H net reaction energy corresponds to the DFT calculated energy of $C_2H_6O_2$ (g) → $HOCH_2CH_2O^*$ + H* reaction.

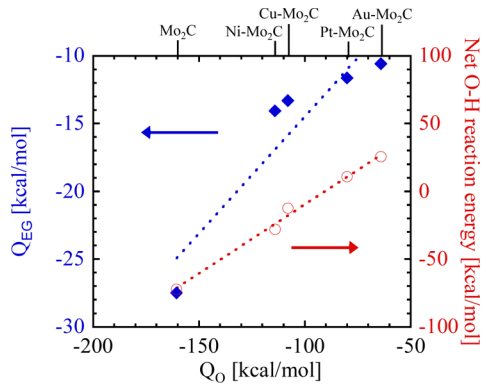

Figure 1. DFT calculated molecular heat of chemisorption of ethylene glycol (Q_{EG}) on M−Mo_2C surfaces (blue diamonds, left axis) and net energy of reaction of O−H scission ($C_2H_6O_2$ (g) → $HOCH_2CH_2O^*$ + H*) (red circles, right axis) as a function of atomic heat of chemisorption of oxygen (Q_O). M−Mo_2C surfaces corresponding to each data series are labeled at the top of graph. Dotted lines are linear regressions to guide the eye.

Figure 2A shows the DFT optimized structure of ethylene glycol adsorbed onto the Ni-modified Mo_2C surface. Figure 2A shows that because of periodic interactions between hydroxyl groups, there is slight deformation of one of the hydroxyl groups compared with adsorption at lower coverage.[15] This periodic

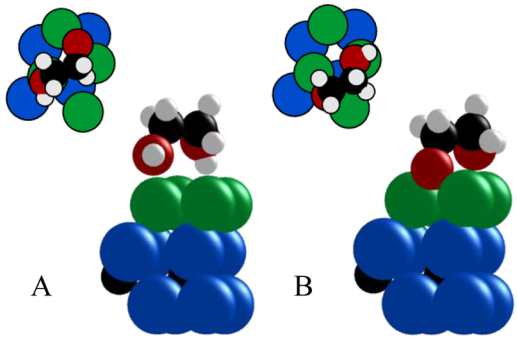

Figure 2. Schematics of (A) ethylene glycol and (B) 2-hydroxyethoxy adsorption on the Ni−Mo_2C surface. Only the top three layers of Mo_2C are shown. Insets show the top view of the adsorbate structure with only the top layer of Mo. Mo, C, O, H, and Ni are represented by blue, black, red, white, and green circles, respectively.

dx.doi.org/10.1021/cs500124n | ACS Catal. 2014, 4, 1409−1418

interaction of hydroxyl groups results in a slight stabilization, evidenced by an ethylene glycol binding energy that is 2.1 kcal/mol stronger on the 2 × 2 slab than the 4 × 4 slab of Mo_2C (not shown). This is consistent with the hydrogen bonding interaction model included in the TPD microkinetic model for this work (see Computational Methods). Figure 2B shows the DFT optimized structure of the O−H bond scission product of ethylene glycol ($HOCH_2CH_2O^*$) on the Ni−Mo_2C surface.

According to Table 1, the predicted TPD activity of ethylene glycol on the Pt(111) surface is 0.037, lower than that on the Ni−Pt(111) surface at 0.154. These numbers are reasonably close to the published TPD experiment data, 0.034 for Pt(111) and 0.167 for Ni−Pt(111) surfaces.[3] Among the admetal modified surfaces, monolayer Ni-modified Mo_2C is the only surface predicted to show higher reforming activity than Ni−Pt(111) surface, followed by Pt- and Cu-modified Mo_2C surfaces. A Au-modified Mo_2C surface is predicted to be inert for the ethylene glycol reaction.

The clean Mo_2C surface is predicted to present high activity (0.250); however, only a very small fraction of ethylene glycol shows reforming activity (0.003). Carbon (C*) formation through complete decomposition and ethylene production from selective deoxygenation makes up the balance on this surface. This implies that unlike the metal and metal-modified surfaces which are favorable to reforming, C−O bond breaking is occurring on the Mo_2C surface. Further investigation of the selectivity of deoxygenation and reforming pathways of ethylene glycol on the Mo_2C surface is illustrated in Section 3.2 through detailed DFT calculations.

3.2. DFT Insights into Selectivity of Reaction Pathways. Expanding on the different product selectivity observed on Mo_2C vs metal-modified Mo_2C, Figure 3 shows the model-predicted steady state selectivity of carbon-containing products from ethylene glycol decomposition as a function of carbon and oxygen atomic binding energies (CSTR design equation was applied to the previously described semiempirical microkinetic model). As shown in Figure 3A, the selectivity toward reforming products (namely CO) is prevalent at the combinations of relatively low atomic oxygen and strong carbon binding energies. On the basis of the calculated atomic oxygen and carbon-binding energies summarized in Table 1, the monolayer Ni-modified Mo_2C and Ni−Pt surfaces are within the high reforming selectivity region, which is consistent with the result predicted by the TPD kinetic model.

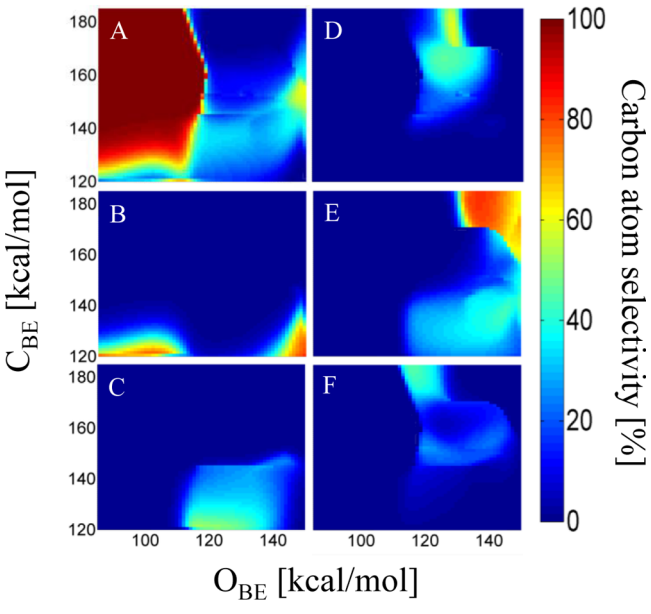

Figure 3. Selectivity toward carbon atom containing products from ethylene glycol decomposition toward (A) CO, (B) $HOCH_2CHO$, (C) CH_3CHO, (D) C_2H_6, (E) C_2H_4, and (F) CH_4 as a function of carbon and oxygen atomic binding energies. Hydrogen binding energy was fixed to the Pt value (56 kcal/mol). CSTR reactor conditions consisted of a temperature of 523 K, total pressure of 1 atm, and a 5% feed of ethylene glycol with the balance He. CH_3OH, C_2H_5OH, and CH_2O (which are negligible) and CO_2 product selectivities (which can contribute up to 40%) are not shown.

In contrast, the strong atomic oxygen and carbon binding energies lead to hydrocarbon products (specifically ethylene in Figure 3E). Strong affinities for oxygen and carbon are characteristic of metal carbide catalysts[30] such as Mo_2C, which is in agreement with the model prediction that the clean Mo_2C surface presents high activity but with low reforming selectivity. To drill down on the unique selectivity observed on bare Mo_2C, competing reaction pathways for reforming and deoxygenation of ethylene glycol were studied via DFT on the β-Mo_2C(0001) surface. This set of DFT calculations provides a better understanding of the elementary reactions controlling the selectivity observed experimentally.

Table 2 displays the energies of intermediate states in the decomposition of ethylene glycol on Mo_2C. DFT-optimized structures of these intermediates are depicted in Supporting Information (SI) Figure S1. Ethylene glycol adsorbs onto the Mo_2C surface with a binding energy of 24.68 kcal/mol (depicted in SI Figure S1A). This is nearly double the binding energy of ethylene glycol on Pt,[15] which is consistent with the stronger atomic oxygen binding energy on Mo_2C.

Table 2. Energetics of Select Ethylene Glycol Decomposition Intermediates on β-Mo_2C(0001) Calculated via DFT

net product	$E - E_0$ (kcal/mol)	figure index
$C_2H_6O_2$ (g)	0.0	
$HOCH_2CH_2OH^*$	−24.68	SI S1A
$HOCH_2CH_2O^* + H^*$	−69.41	SI S1B
$OCH_2CH_2O^* + 2H^*$	−115.31	SI S1C
$HOCH_2CHO^* + 2H^*$	−89.25	SI S1D
$OCH_2CHO^* + 3H^*$	−121.76	SI S1E
$HOCH_2CO^* + 3H^*$	−93.63	SI S1F
$OCH_2CO^* + 4H^*$	−124.53	SI S1G
$HOCH_2CH_2^* + O^* + H^*$	−110.23	SI S1H
$OCH_2CH_2^* + O^* + 2H^*$	−152.20	SI S1I
$CH_2CH_2^* + 2O^* + 2H^*$	−195.79	SI S1J

Net product refers to $C_2H_xO_2$ intermediate resulting from ethylene glycol decomposition with excess O* and H* adsorbed on separate slabs. $E - E_0$ refers to the net DFT reaction energy from gas-phase ethylene glycol to this state. The final column is the index of the intermediate depicted in SI Figure S1.

In addition, as the energetic values show in Table 2, decomposition energetically favors the maximization of oxygen−surface interactions. O−H bond cleavage products on Mo_2C are typically 23−46 kcal/mol more stable than those resulting from alcohol reactants. Alkoxide intermediates bind to the C-vacant 3-fold sites (see SI Figure S1B, C, E, G, and I). Alkoxide adsorption on this site is typically 2−5 kcal/mol more stable than adsorption to a top site. The C−O bond cleaving reactions are also highly exothermic (reaction energies from −23

dx.doi.org/10.1021/cs500124n | ACS Catal. 2014, 4, 1409−1418

to −46 kcal/mol). A more complete understanding of kinetic trends is gained through the comparison of transition state energetics. Table 3 shows the DFT calculated reaction energies and activation barriers of competing O−H, C−H, and C−O bond cleaving reactions for ethylene glycol intermediates on Mo_2C. DFT optimized transition state structures for O−H, C−O, and C−H cleaving reactions are depicted in SI Figures S2−S4, respectively. Upon adsorption, $HOCH_2CH_2OH^*$ undergoes rapid O−H scission to form the alkoxide $HOCH_2CH_2O^*$ (shown in SI Figure S2A). This highly exothermic reaction proceeds with a barrier of only 1.61 kcal/mol. The most favorable reaction for $HOCH_2CH_2O^*$ is a second O−H bond scission forming $OCH_2CH_2O^*$ (shown in SI Figure S2B). This reaction carries a barrier of 6.23 kcal/mol compared with barriers of 19.37 and 8.53 kcal/mol for C−O and C−H bond scission, respectively. This is consistent with previous surface science experiments that carbide surfaces are extremely active for O−H bond cleavage, even at low temperatures.[31]

Table 3. DFT Calculated Reaction Energies and Activation Barriers for Select Decomposition Reactions of $C_2H_xO_2$ Species on Mo_2C

reaction	ΔE (kcal/mol)	$\Delta E^{\ddagger}$ (kcal/mol)	figure index
$C_2H_6O_2$ (g) → $HOCH_2CH_2OH^*$	−24.68		
C_2H_4 (g) → $CH_2CH_2^*$	−45.66		
O−H Bond Breaking			
$C_2H_6O_2^*$ → $HOCH_2CH_2O^*$ + H*	−41.97	1.61	SI S2A
$HOCH_2CH_2O^*$ → $OCH_2CH_2O^*$ + H*	−48.66	6.23	SI S2B
$HOCH_2CHO^*$ → OCH_2CHO^* + H*	−32.75	15.68	SI S2C
C−O Bond Breaking			
$HOCH_2CH2O^*$→ $CH_2CH_2OH^*$ + O*	−40.82	19.37	SI S3A
$OCH_2CH_2O^*$ → $CH_2CH_2O^*$ + O*	−36.90	19.37	SI S3B
$HOCH_2CHO^*$ → $CHCH_2OH^*$ + O*	−30.67	11.07	SI S3C
OCH_2CHO^* → $CHCH_2O^*$ + O*	−41.97	17.07	SI S3D
$CH_2CH_2OH^*$ → $CH_2CH_2^*$ + OH*	−53.04	3.23	SI S3E
$CH_2CH_2O^*$ → $CH_2CH_2^*$ + O*	−43.59	5.30	SI S3F
C−H Bond Breaking			
$HOCH_2CH_2O^*$ → $HOCH_2CHO^*$ + H*	−22.37	8.53	SI S4A
$OCH_2CH_2O^*$ → OCH_2CHO^* + H*	−6.46	25.60	SI S4B
$HOCH_2CHO^*$ → $HOCH_2CO^*$ + H*	−4.38	22.60	SI S4C
OCH_2CHO^* → OCH_2CO^* + H*	−2.54	30.21	SI S4D

ΔE represents DFT calculated reaction energies. Product species are adsorbed on separate slabs. $\Delta E^{\ddagger}$ represents DFT calculated activation energies.

The O−H bond breaking reactions are highly favorable both thermodynamically and kinetically. Upon formation of the $OCH_2CH_2O^*$ intermediate, competition exists between C−H bond cleaving and C−O bond cleaving reactions. C−O bond breaking of $OCH_2CH_2O^*$ to $CH_2CH_2O^*$ (SI Figure S3B) requires a barrier of only 19.37 kcal/mol, compared with a 25.60 kcal/mol barrier for C−H cleavage to OCH_2CHO^* (SI Figure S4B). Subsequent C−O scission of $CH_2CH_2O^*$ to ethylene requires a barrier of only 5.30 kcal/mol (SI Figure S3F). Important to note is that the transition state structure for this final C−O cleaving reaction (shown in SI Figure S3F) positions the ethylene fragment in a more weakly adsorbed state (similar to π-adsorbed ethylene[32]). This suggests that ethylene may not be fully adsorbed before desorbing upon formation from deoxygenation of $CH_2CH_2O^*$. This likely improves the selectivity of ethylene compared with ethane due to desorption being increasingly favorable to hydrogenation.

These trends are in reasonable agreement with a recently published article focused on the decomposition of ethanol on an α-$Mo_2C(100)$ surface.[33] Although the reaction energies for O−H and C−O bond scission are more favorable in the present study, most likely due to the strong affinity to oxygen of the C-vacant 3-fold site on the β-$Mo_2C(0001)$ surface, the same general trend is observed in the work by Xing and Wang for ethanol decomposition, with the O−H bond scission being favored to C−H bond scission for ethanol. After dehydrogenation, C−O bond scission reactions become most favorable, while C−C bond scission pathways have high barriers (typically >23 kcal/mol). It is also agreed that the most likely pathway to form ethylene involves the C−O bond scission of the $CH_2CH_2O^*$ intermediate.

Previous research has emphasized the importance of C−C vs C−O bond-cleaving reactions as key to reforming vs HDO selective catalysts.[34−37] Although certainly intuitive from macroscopic considerations, at the elementary reaction level, which can weigh more heavily into catalyst design considerations,[12,38] producing ethylene from ethylene glycol hinges on cleaving O−H and C−O bonds in alkoxide species more selectively than C−H bonds (which could eventually lead to acetyl intermediates that undergo C−C cleaving[29]).

This notion of divergent pathways at alkoxide intermediates is supported by past research from Goodman and co-workers, who determined that hydrocarbon formation from ethanol on Pd(110) occurs from C−O cleavage of the ethoxy species

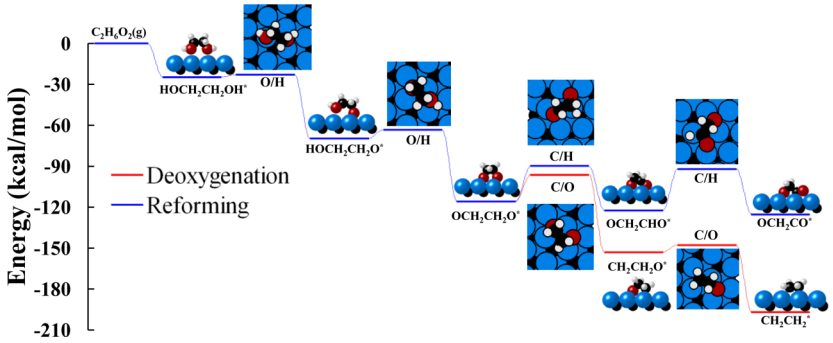

Figure 4. DFT calculated energy profile of favorable deoxygenation vs reforming reaction pathways of ethylene glycol on Mo_2C.

dx.doi.org/10.1021/cs500124n | ACS Catal. 2014, 4, 1409−1418

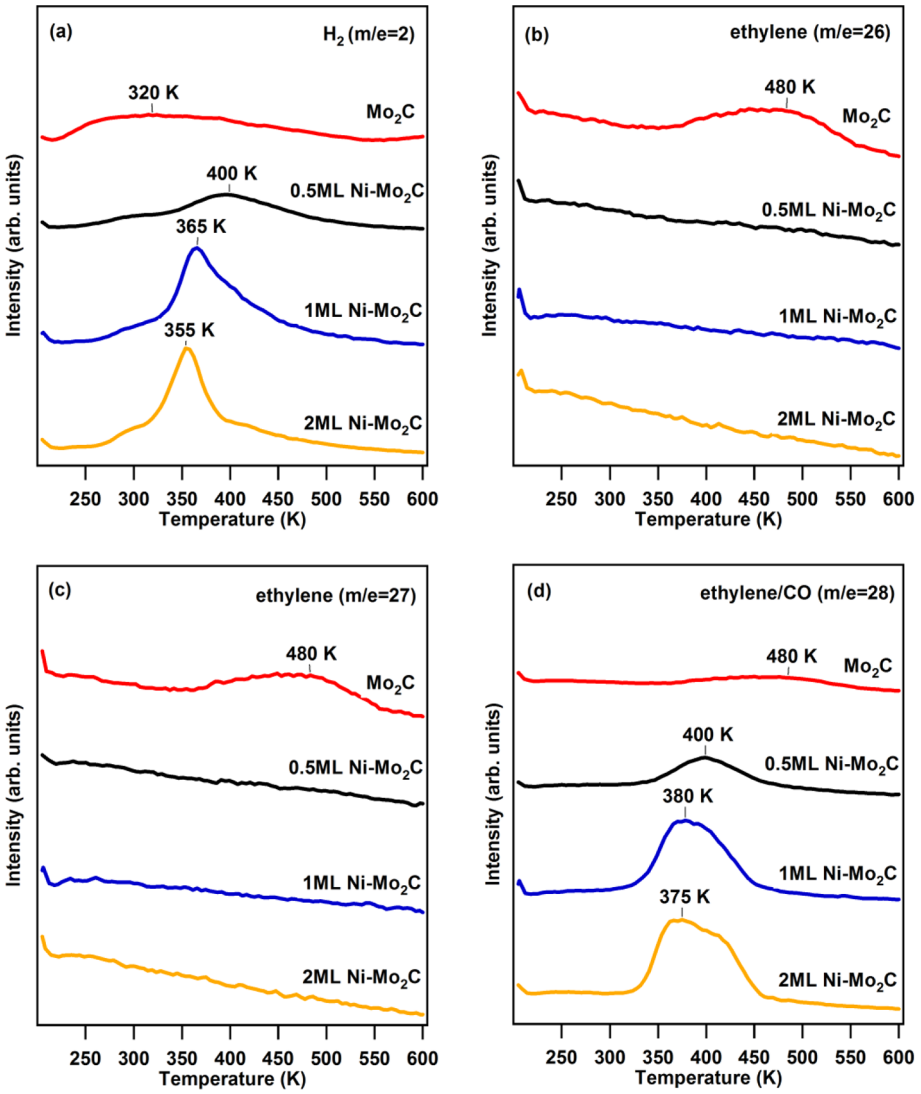

Figure 5. TPD spectra of (a) H_2, (b) C_2H_4 ($m/e = 26$), (c) C_2H_4 ($m/e = 27$) and (d) C_2H_4/CO ($m/e = 28$) following 4 L exposure of ethylene glycol on Mo_2C and Ni−Mo_2C surfaces.

(albeit, most likely, at defect sites).[39] This competition is illustrated in Figure 4, which shows after a facile completion of O−H bond cleaving, the most favorable pathways for further decomposition are either C−H bond breaking (shown in blue) or C−O bond breaking (shown in red). According to the DFT results shown in Table 3, the barrier for C−O bond breaking is ∼7 kcal/mol lower than the competing C−H breaking, which could lead the reaction of ethylene glycol on Mo_2C surface following the deoxygenation pathway to produce ethylene with the favorable C−O bond breaking.

3.3. Selectivity and Activity of Ethylene Glycol from TPD Experiments on Mo_2C and M−Mo_2C Surfaces. Three possible net reaction pathways of ethylene glycol are summarized as follows:

$$a\ C_2H_6O_2 \rightarrow 2a\ C_{(ad)} + 2a\ O_{(ad)} + 3a\ H_2 \quad (1)$$

$$b\ C_2H_6O_2 \rightarrow b\ C_2H_4 + 2b\ O_{(ad)} + b\ H_2 \quad (2)$$

$$c\ C_2H_6O_2 \rightarrow 2c\ CO + 3c\ H_2 \quad (3)$$

Reaction 1 represents the total decomposition pathway, in which all of the C−C, C−O, C−H, and O−H bonds in ethylene glycol break to produce hydrogen, as well as C_{ad} and O_{ad}. The accumulation of C_{ad} and O_{ad} on the surface will deactivate the catalyst surface. Reaction 2 is the deoxygenation pathway that selectively dissociates the two C−O bonds to produce ethylene, hydrogen, and O_{ad}. Reaction 3 is the reforming pathway involving the C−C bond scission and C−O bonds intact, which is the most desirable pathway because it produces syngas. Here, values of a, b, and c in the equations represent the amount of chemisorbed ethylene glycol molecules that undergo each reaction pathway.

Ethylene glycol TPD experiments were performed on clean Mo_2C and different metal-modified Mo_2C surfaces. Figure 5 displays the TPD spectra of reaction products H_2, C_2H_4, and CO following 4 L ethylene glycol on Mo_2C and Ni-modified Mo_2C surfaces. In Figure 5a, a broad hydrogen desorption peak is observed on the clean Mo_2C surface around 320 K. When the surface is modified by Ni layers, hydrogen is found to desorb at 400 K from the 0.5 ML Ni−Mo_2C surface, 365 K from the 1 ML Ni−Mo_2C surface, and 355 K from the 2 ML Ni−Mo_2C surface. On the clean Mo_2C surface, a desorption peak at the same temperature (480 K) is detected at m/e = 26, 27, and 28, which are the cracking fragments of ethylene. The combination of

dx.doi.org/10.1021/cs500124n | ACS Catal. 2014, 4, 1409−1418

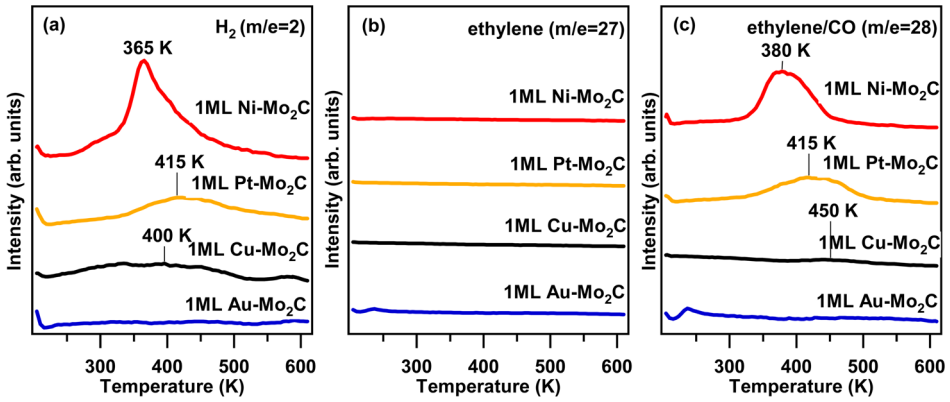

Figure 6. TPD spectra of (a) H_2, (b) C_2H_4 (m/e = 27) and (c) C_2H_4/CO (m/e = 28) following 4 L exposure of ethylene glycol on monolayer metal-modified Mo_2C surfaces.

Table 4. Reactivity of Ethylene Glycol on Mo_2C and Modified Mo_2C Surfaces

	activity (molecule per metal atom)			
surface	complete decomposition (a)	deoxygenation (b)	reforming (c)	total
Mo_2C	0.092	0.069	0.000	0.161
0.5 ML Ni−Mo_2C	0.063	0.000	0.069	0.132
1 ML Ni−Mo_2C	0.064	0.000	0.162	0.227
2 ML Ni−Mo_2C	0.027	0.000	0.098	0.125
0.5 ML Au−Mo_2C	0.000	0.000	0.000	0.000
1 ML Au−Mo_2C	0.000	0.000	0.000	0.000
2 ML Au−Mo_2C	0.000	0.000	0.000	0.000
0.5 ML Cu−Mo_2C	0.021	0.010	0.000	0.031
1 ML Cu−Mo_2C	0.054	0.000	0.001	0.055
2 ML Cu−Mo_2C	0.021	0.000	0.003	0.024
0.5 ML Pt−Mo_2C	0.044	0.000	0.011	0.056
1 ML Pt−Mo_2C	0.016	0.000	0.060	0.076
2 ML Pt−Mo_2C	0.000	0.000	0.042	0.042

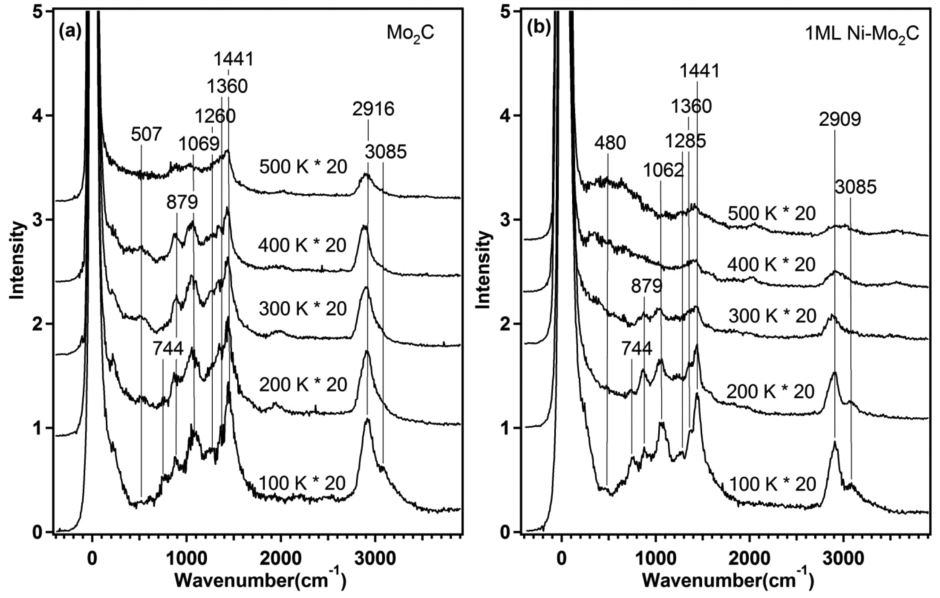

Figure 7. HREEL spectra of 4 L ethylene glycol on (a) Mo_2C surface and (b) 1 ML Ni−Mo_2C surface.

desorption peaks in Figure 5b, c, and d indicates that ethylene glycol follows the deoxygenation pathway on the Mo_2C surface with C−O bond scission to produce ethylene. No desorption peak is observed at m/e = 26 and 27 for Ni-modified Mo_2C surfaces. In Figure 5d, the desorption peaks at m/e = 28 indicate the CO product desorbs from the 0.5 ML Ni−Mo_2C surface at 400 K, from the 1 ML Ni−Mo_2C surface at 380 K, and from the 2 ML Ni−Mo_2C surface at 375 K. Unlike on clean Mo_2C, on the

dx.doi.org/10.1021/cs500124n | ACS Catal. 2014, 4, 1409−1418

Ni-modified Mo_2C surfaces, H_2 and CO are identified as reaction products from the total decomposition and reforming pathways.

Similar TPD measurements on other metal-modified Mo_2C surfaces are shown in SI Figures S5 (Au), S6 (Cu), and S7 (Pt) at different metal coverages. The TPD spectra from ethylene glycol reaction on the ML coverage of the four metal (Ni, Pt, Au, and Cu)-modified Mo_2C surfaces are compared in Figure 6, which shows that H_2 and CO are the main products from ethylene glycol from all surfaces. Among the four surfaces, 1 ML Ni−Mo_2C shows the highest H_2 and CO desorption peak areas, followed by the ML Pt-, Cu-, and Au-modified Mo_2C surfaces, indicating the activity of ethylene glycol follows the trend of Ni−Mo_2C > Pt−Mo_2C > Cu−Mo_2C > Au−Mo_2C.

The TPD experiments of ethylene glycol are quantified using the product desorption peak areas with the appropriate subtraction of background contribution. The detail quantification method of TPD experiment has been described in previous studies.[25,26] The quantification results of the ethylene glycol reaction activity on clean Mo_2C and different metal-modified Mo_2C surfaces are shown in Table 4. According to Table 4, on the clean Mo_2C surface, ethylene glycol undergoes the total decomposition (0.092) and deoxygenation (0.069) pathways. There is no experimental reforming activity of ethylene glycol from the Mo_2C surface, similar to the reforming activity prediction in Table 1. Among all the metal-modified Mo_2C surfaces, ML Ni−Mo_2C surface displays the highest total activity (0.227), followed by ML Pt−Mo_2C (0.076), ML Cu−Mo_2C (0.055), and ML Au−Mo_2C (0.000) surfaces.

3.4. Selectivity of Ethylene Glycol from HREELS Experiments on Mo_2C and 1 ML Ni−Mo_2C Surfaces. HREELS experiments were carried out to monitor the surface reaction intermediates from ethylene glycol decomposition on the clean Mo_2C surface (Figure 7a) and 1 ML Ni−Mo_2C surface (Figure 7b). The HREEL spectrum on clean Mo_2C at 100 K exhibits the following characteristic vibrational modes of molecularly adsorbed ethylene glycol, as assigned in SI Table S1:[2,40] δ(CCO), 507 cm^{-1}; τ(OH), 744 cm^{-1}; ν(CC), $\rho_r(CH_2)$, 879 cm^{-1}; ν_s(CO), 1069 cm^{-1}; $\rho_t(CH_2)$, 1260 cm^{-1}; $\rho_w(CH_2)$, 1360 cm^{-1}; $\delta(CH_2)$, 1441 cm^{-1}; ν_{as}(CH), 2916 cm^{-1}; ν(OH), 3085 cm^{-1}. The vibrational frequencies observed in the HREELS experiment are consistent with those calculated using DFT, as shown in SI Table S1. No obvious change is observed in the HREEL spectrum upon heating to 200 K, indicating that ethylene glycol is still molecularly adsorbed on the Mo_2C surface with the O−H bond intact. After heating to 300 K, both the τ(OH) mode at 744 cm^{-1} and ν(OH) at 3085 cm^{-1} disappear, indicating that the O−H bond cleavage occurs between 200 and 300 K to produce an ethylenedioxy (OCH_2CH_2O) intermediate. The ethylenedioxy intermediate remains intact on the Mo_2C surface at 400 K, similar to the adsorption study of ethanol on Mo_2C with the C−C bond intact.[41] After heating the surface to 500 K, all of the vibrational modes are still present, but with a considerable decrease in intensity, consistent with the TPD result that the ethylene product is produced between 400 and 600 K.

Figure 7b shows the HREEL spectra of 4 L ethylene glycol dosed on the 1 ML Ni−Mo_2C surface. The HREEL spectrum at 100 K shows the characteristic vibrational modes of molecularly adsorbed ethylene glycol. Compared with clean Mo_2C surface, the main difference is the disappearance of the ν(CC) mode at 879 cm^{-1} after 300 K, indicating that on the 1 ML Ni−Mo_2C surface, ethylene glycol follows the C−C bond scission to produce H_2 and CO after 300 K, consistent with the TPD results.

4. DISCUSSION

4.1. Correlating Ethylene Glycol Activity from Model Prediction to TPD Experimental Results. As shown in Section 3.3, ethylene glycol shows deoxygenation and total decomposition activities on the Mo_2C surface, but not reforming activity. This loss in reforming selectivity on the bare Mo_2C surface can be explained by the high carbon, oxygen, and hydrogen binding energies on β-Mo_2C(0001), which leads to more favorable deoxygenation than reforming, as shown in Section 3.2. C−O bond cleaving exhibits a lower barrier than C−H bond breaking (Figure 4). The high C−O bond cleaving activity of the Mo_2C surface enables fast ethylene formation and prevents further dehydrogenation, which can lead to reforming products.

In contrast, when the surface is modified by various metals, ethylene glycol undergoes the dehydrogenation and eventual C−C bond scission for total decomposition and reforming pathways. One exception is the 0.5 ML Cu−Mo_2C surface, which still presents a low total deoxygenation (0.01) activity to produce ethylene. It is possible that when half of the surface is covered by Cu, the uncovered portion of the surface still exhibits some property of bare Mo_2C for deoxygenation activity with C−O cleavage. Among all the metal-modified Mo_2C surfaces, the 1 ML $NiMo_2C$ surface displays the highest reforming activity and total activity, followed by Pt- and Cu-modified surfaces. This is not surprising given the similarity in atomic binding energies of Ni−Mo_2C to the Ni/Pt bimetallic catalyst that has been previously identified as an active reforming catalyst for oxygenates.[2,3,11,28,29] Au-modified Mo_2C surfaces are inert for the ethylene glycol reactions. The trend in the experimental quantification result generally agrees with the one from the theoretical prediction, as shown in Figure 8.

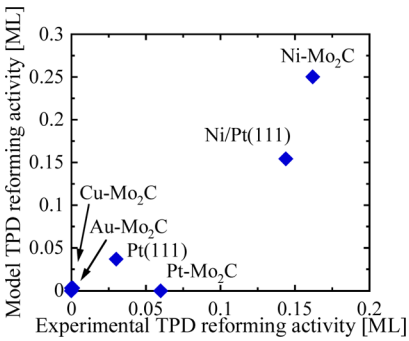

Figure 8. Comparison of ethylene glycol decomposition experimental TPD reforming activity with model results.

The trend in the experimental quantification result generally agrees with the one from the theoretical prediction, as shown in Figure 8. A balance exists in the TPD model between the ethylene glycol desorption rate and the initial hydrogen extraction reaction rate. For surfaces with weak atomic oxygen binding energy, the desorption rate of ethylene glycol is faster than the rate for initial dehydrogenation. This is true for the Au−Mo_2C and Pt−Mo_2C monolayer carbide surfaces, which show very little activity (see Table 1). The Cu−Mo_2C and Pt(111) surfaces begin to show some activity as the oxygen binding energy increases. However, in the case of Cu−Mo_2C, the low hydrogen binding energy contributes to a higher barrier for initial dehydrogenation when viewed through the barrier calculation by linear free energy relationships. The most active reforming

dx.doi.org/10.1021/cs500124n | ACS Catal. 2014, 4, 1409−1418

catalysts are the Ni/Pt(111) surface and the Ni−Mo_2C surfaces, which actively and selectively decompose ethylene glycol to CO (Ni/Pt shows over 99% selectivity to reforming products). As a side note, it is possible that some of the loss in reforming selectivity of the Ni−Mo_2C surface can be attributed to exposed Mo_2C surface. Further, as the atomic oxygen binding energy increases past the optimal reforming catalyst, TPD selectivity converts to C−O bond breaking products (either ethylene or adsorbed carbon and oxygen). This is the case for the bare Mo_2C surface.

4.2. Correlating Ethylene Glycol Selectivity from Model Prediction to TPD and HREELS Experimental Results. The progression from ethylene glycol to reforming or deoxygenation products through varying elementary reaction pathways is shown in the schematic in Figure 9. After decomposition initiates

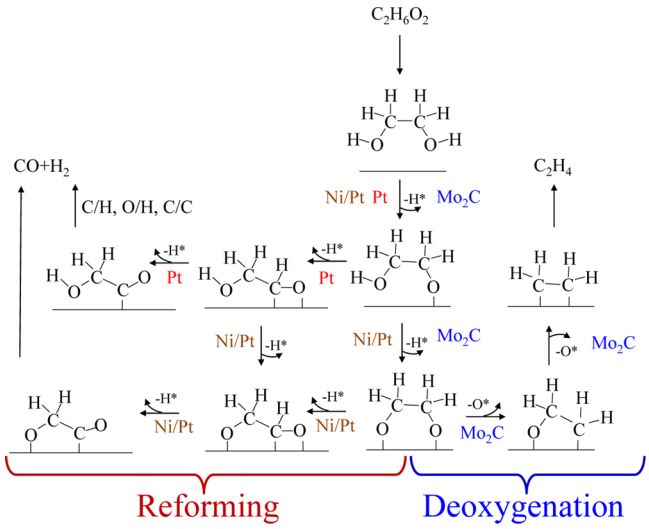

Figure 9. Schematic of elementary reactions controlling reforming vs HDO mechanisms for ethylene glycol-derived intermediates. Here, the Mo_2C surface is compared with previously studied Pt-based reforming catalysts.[29]

through initial O−H bond breaking, the subsequent pathways vary on the basis of the relative activities of the competing elementary reactions. On the Pt surface, which has the lowest affinity for oxygen, reforming proceeds through C−H bond cleaving to form surface glycolaldehyde.[29] Ensuing dehydrogenation and C−C bond cleaving then lead to CO and H_2 products.[28,29] On the Ni/Pt surface (which is expected to behave similarly to the Ni−Mo_2C surface) where reforming activity is approximately maximized, an increased affinity for oxygen leads to a favorable pathway for ethylenedioxy (OCH_2CH_2O*) formation.[29] For these Ni monolayer surfaces, C−H bond cleaving is most favorable from OCH_2CH_2O*, which eventually leads to reforming products. Finally, as the atomic binding energies increase past the optimal reforming catalysts, as is the case for Mo_2C, C−O scission of the OCH_2CH_2O* intermediate becomes preferred to C−H scission. Subsequent deoxygenation is facile from the CH_2CH_2O* intermediate (see Figure 4). This diagram (Figure 9) summarizes the competition between C−H scission and C−O scission reactions, which control the observed selectivity of reforming vs deoxygenation products for ethylene glycol decomposition, as demonstrated with the TPD experiments of Mo_2C and metal-modified Mo_2C surfaces in this work.

On the basis of the microkinetic model, ethylene glycol follows the deoxygenation pathway on surfaces with too strong affinity for oxygen, such as the Mo_2C surface, and follows the reforming pathway on surfaces with optimal oxygen binding energy, such as the Ni-modified Mo_2C surface. This is consistent with the TPD results that ethylene glycol produces ethylene on the Mo_2C surface and syngas (H_2 and CO) on metal-modified Mo_2C surfaces. The selectivity predicted in the model is further verified with the HREELS results on Mo_2C and 1 ML Ni−Mo_2C surfaces. According to Section 3.4, on the clean Mo_2C surface, which has a very strong oxygen-binding energy, ethylene glycol produces ethylene due to the presence of the stable ethylenedioxy species at 400 K. In contrast, on the 1 ML Ni−Mo_2C surface with an optimal affinity for oxygen, ethylene glycol follows the reforming pathway, with C−C bond scission occurring between 300 and 400 K to produce H_2 and CO. The selectivity prediction of ethylene glycol based on the oxygen binding energy is confirmed using the TPD and HREELS experimental results.

5. CONCLUSIONS

A methodology for catalyst design and for understanding the underlying mechanisms governing product selectivity is established in this work by the combination of a microkinetic model and parallel TPD and HREELS experiments. A semi-empirically based microkinetic model is modified to predict the reaction activity and selectivity of ethylene glycol on clean Mo_2C and different metal (Ni, Au, Cu, and Pt)-modified Mo_2C surfaces. The strong atomic carbon and oxygen binding energies on the clean Mo_2C surface lead to high C−O bond cleavage selectivity, and thus ethylene glycol follows the deoxygenation and complete decomposition pathways. When the Mo_2C surface is modified by other metals (Ni, Pt, Au, and Cu), the lower oxygen atomic binding energies cause ethylene glycol to follow the reforming pathway. Among the metal-modified surfaces, monolayer Ni-modified Mo_2C surface shows the highest reforming activity. The predicted reforming activity trend is experimentally confirmed by TPD quantification results, and the reaction selectivity prediction is verified by the TPD and HREELS experimental results. The methodology for catalyst design in the current study should provide a guide for future catalyst discovery for other catalytic reactions.

■ ASSOCIATED CONTENT

Supporting Information

Additional structural and energetic information on the DFT calculated transition states and intermediates. TPD spectra from the decomposition of ethylene glycol on Mo_2C, Au−Mo_2C, Cu−Mo_2C, and Pt−Mo_2C surfaces. Vibrational assignment for adsorbed ethylene glycol on clean Mo_2C surface. This material is available free of charge via the Internet at http://pubs.acs.org/.

■ AUTHOR INFORMATION

Corresponding Authors

*E-mail: vlachos@udel.edu.
*E-mail: jgchen@columbia.edu

Notes

The authors declare no competing financial interest.

■ ACKNOWLEDGMENTS

This article was based on work supported as part of the Catalysis Center for Energy Innovation (CCEI), an Energy Frontier

Research Center (EFRC) funded by the U.S. Department of Energy, Office of Science, Office of Basic Energy Sciences under Award No. DE-SC0001004.

REFERENCES

(1) Ji, N.; Zhang, T.; Zheng, M. Y.; Wang, A. Q.; Wang, H.; Wang, X. D.; Chen, J. G. *Angew. Chem., Int. Ed.* **2008**, *47* (44), 8510−8513.
(2) Skoplyak, O.; Barteau, M. A.; Chen, J. G. *Surf. Sci.* **2008**, *602* (23), 3578−3587.
(3) Skoplyak, O.; Barteau, M. A.; Chen, J. G. *J. Phys. Chem. B* **2006**, *110* (4), 1686−1694.
(4) Menning, C. A.; Chen, J. G. *J. Chem. Phys.* **2009**, *130* (17), 174709.
(5) Kitchin, J. R.; Khan, N. A.; Barteau, M. A.; Chen, J. G.; Yakshinksiy, B.; Madey, T. E. *Surf. Sci.* **2003**, *544* (2−3), 295−308.
(6) Oyama, S. T. *The Chemistry of Transition Metal Carbides and Nitrides*; Blackie Academic & Professional: Glasgow, 1996.
(7) Hwu, H. H.; Chen, J. G. *Chem. Rev.* **2005**, *105* (1), 185−212.
(8) Levy, R. B.; Boudart, M. *Science* **1973**, *181* (4099), 547−549.
(9) Esposito, D. V.; Hunt, S. T.; Stottlemyer, A. L.; Dobson, K. D.; McCandless, B. E.; Birkmire, R. W.; Chen, J. G. *Angew. Chem., Int. Ed.* **2010**, *49* (51), 9859−9862.
(10) Ren, H.; Yu, W.; Salciccioli, M.; Chen, Y.; Huang, Y.; Xiong, K.; Vlachos, D. G.; Chen, J. G. *ChemSusChem* **2013**, 798−801.
(11) Salciccioli, M.; Vlachos, D. G. *ACS Catal.* **2011**, *1* (10), 1246−1256.
(12) Salciccioli, M.; Stamatakis, M.; Caratzoulas, S.; Vlachos, D. G. *Chem. Eng. Sci.* **2011**, *66* (19), 4319−4355.
(13) Abild-Pedersen, F.; Greeley, J.; Studt, F.; Rossmeisl, J.; Munter, T. R.; Moses, P. G.; Skulason, E.; Bligaard, T.; Nørskov, J. K. *Phys. Rev. Lett.* **2007**, *99* (1), 016105.
(14) Jones, G.; Bligaard, T.; Abild-Pedersen, F.; Nørskov, J. K. *J. Phys.: Condens. Matter* **2008**, *20* (6), 064239.
(15) Salciccioli, M.; Chen, Y.; Vlachos, D. G. *J. Phys. Chem. C* **2010**, *114* (47), 20155−20166.
(16) Kresse, G.; Hafner, J. *Phys. Rev. B* **1993**, *47* (1), 558−561.
(17) Kresse, G.; Furthmuller, J. *Phys. Rev. B* **1996**, *54* (16), 11169−11186.
(18) Kitchin, J. R.; Nørskov, J. K.; Barteau, M. A.; Chen, J. G. *Catal. Today* **2005**, *105* (1), 66−73.
(19) Perdew, J. P.; Wang, Y. *Phys. Rev. B* **1992**, *45* (23), 13244−13249.
(20) Perdew, J. P.; Burke, K.; Ernzerhof, M. *Phys. Rev. Lett.* **1996**, *77* (18), 3865−3868.
(21) Kresse, G.; Joubert, D. *Phys. Rev. B* **1999**, *59* (3), 1758−1775.
(22) Henkelman, G.; Jonsson, H. *J. Chem. Phys.* **1999**, *111* (15), 7010−7022.
(23) Alavi, A.; Hu, P. J.; Deutsch, T.; Silvestrelli, P. L.; Hutter, J. *Phys. Rev. Lett.* **1998**, *80* (16), 3650−3653.
(24) Michaelides, A.; Liu, Z. P.; Zhang, C. J.; Alavi, A.; King, D. A.; Hu, P. *J. Am. Chem. Soc.* **2003**, *125* (13), 3704−3705.
(25) Yu, W. T.; Barteau, M. A.; Chen, J. G. *J. Am. Chem. Soc.* **2011**, *133* (50), 20528−20535.
(26) Hwu, H. H.; Chen, J. G. *Surf. Sci.* **2003**, *536* (1−3), 75−87.
(27) Cumpson, P. J.; Seah, M. P. *Surf. Interface Anal.* **1997**, *25* (6), 430−446.
(28) Salciccioli, M.; Vlachos, D. G. *J. Phys. Chem. A* **2012**, *116* (18), 4621−4628.
(29) Salciccioli, M.; Yu, W.; Barteau, M. A.; Chen, J. G.; Vlachos, D. G. *J. Am. Chem. Soc.* **2011**, *133* (20), 7996−8004.
(30) Ren, H.; Hansgen, D. A.; Stottlemyer, A. L.; Kelly, T. G.; Chen, J. G. *ACS Catal.* **2011**, *1* (4), 390−398.
(31) Yu, W. T.; Mellinger, Z. J.; Barteau, M. A.; Chen, J. G. *J. Phys. Chem. C* **2012**, *116* (9), 5720−5729.
(32) Salciccioli, M.; Chen, Y.; Vlachos, D. G. *Ind. Eng. Chem. Res.* **2011**, *50* (1), 28−40.
(33) Xing, S. K.; Wang, G. C. *J. Mol. Catal. A, Chem.* **2013**, *377*, 180−189.
(34) Davda, R. R.; Shabaker, J. W.; Huber, G. W.; Cortright, R. D.; Dumesic, J. A. *Appl. Catal., B* **2005**, *56* (1−2), 171−186.
(35) Chheda, J. N.; Huber, G. W.; Dumesic, J. A. *Angew. Chem., Int. Ed.* **2007**, *46* (38), 7164−7183.
(36) Ferrin, P.; Simonetti, D.; Kandoi, S.; Kunkes, E.; Dumesic, J. A.; Nørskov, J. K.; Mavrikakis, M. *J. Am. Chem. Soc.* **2009**, *131* (16), 5809−5815.
(37) Alcalá, R.; Mavrikakis, M.; Dumesic, J. A. *J. Catal.* **2003**, *218* (1), 178−190.
(38) Nørskov, J. K.; Bligaard, T.; Rossmeisl, J.; Christensen, C. H. *Nat. Chem.* **2009**, *1* (1), 37−46.
(39) Bowker, M.; Holroyd, R. P.; Sharpe, R. G.; Corneille, J. S.; Francis, S. M.; Goodman, D. W. *Surf. Sci.* **1997**, *370* (2−3), 113−124.
(40) Sawodny, W.; Niedenzu, K.; Dawson, J. W. *Spectrochim. Acta, Part A* **1967**, *A 23* (4), 799−806.
(41) Farkas, A. P.; Solymosi, F. *Surf. Sci.* **2007**, *601* (1), 193−200.